Nuclear Inst. and Methods in Physics Research, A 1033 (2022) 166591

Contents lists available at ScienceDirect

Nuclear Inst. and Methods in Physics Research, A

journal homepage: www.elsevier.com/locate/nima

Start-to-end simulations of plasma-wakefield acceleration using the MAX IV Linear Accelerator

J. Björklund Svensson [a,*], J. Andersson [b], J. Ferri [c,d], T.K. Charles [g,f], H. Ekerfelt [a,e], E. Mansten [b], S. Thorin [b], O. Lundh [a]

[a] Department of Physics, Lund University, P.O. Box 118, SE-22100, Lund, Sweden
[b] MAX IV Laboratory, Lund University, P.O. Box 118, SE-22100, Lund, Sweden
[c] Department of Physics, Chalmers University of Technology, SE-41296 Gothenburg, Sweden
[d] Department of Physics, University of Gothenburg, SE-41296, Gothenburg, Sweden
[e] SLAC National Accelerator Laboratory, Menlo Park, CA 94025, USA
[f] The Cockcroft Institute, Daresbury, Warrington WA4 4AD, United Kingdom
[g] Department of Physics, University of Liverpool, Liverpool, United Kingdom

ARTICLE INFO

Keywords:
Plasma-wakefield acceleration
Electrons
MAX IV
Linear accelerator
Simulations

ABSTRACT

Plasma-wakefield acceleration (PWFA) relies on the interaction between intense particle bunches and plasma for reaching higher accelerating gradients than what is possible with conventional radio-frequency technology. Using ultra-relativistic beam drivers allows for long acceleration lengths and have potential applications such as energy booster stages for synchrotron light sources or linear colliders and generating ultra-high-brightness beams from the background plasma. In this article, we present start-to-end simulations of the MAX IV Linear Accelerator as part of our investigations into the feasibility of using the linac for a PWFA experiment. We find that PWFA appears to be a viable application for the linac. A part of this conclusion is based on our finding that the general properties of the bunch compressor type employed in the MAX IV linac are well-suited for efficient generation of PWFA-optimized bunch current profiles, both for single- and double-bunch beams.

1. Introduction

As the interest in using high-energy charged particle beams for various applications has grown, so has the demand for developing more compact sources which can deliver beams of high quality, i.e. high 6D brightness (low emittance, low energy spread, and high peak current), while keeping the required infrastructure to a minimum. Plasma-wakefield acceleration (PWFA) [1,2] is an acceleration scheme with the potential to fulfill these demands. In this scheme, an ultra-relativistic charged particle bunch, typically called the driver bunch, is focused into a plasma. Its Coulomb field laterally expels the plasma electrons, forming a positively charged volume in its wake, with the heavy ions usually remaining stationary on the time scale relevant for PWFA. This positive charge density attracts the expelled electrons, which start performing oscillations around the beam axis. Such a wake structure can sustain extremely strong electromagnetic fields, typically two to three orders of magnitude higher than conventional radio-frequency (RF) structures.

If the driver bunch has a sufficiently high electron density, more than a factor of ~2 higher than the background plasma, and the bunch size is matched to the plasma density, nearly all of the plasma electrons can be expelled from the region behind the driver and form a bare ion cavity [3]. This is usually called the blow-out or bubble regime. In this regime, the transverse electromagnetic force in the bubble has a linear gradient [3], which makes it ideal for accelerating high-quality beams of charged particles since it preserves transverse emittance. Specifically, for negatively charged particles, the transverse force is focusing and accelerating in the rear half of the bubble. This means that a second bunch of electrons, typically called the witness bunch, can gain a substantial amount of energy, if injected at an appropriate phase in the wake. Injection of the witness bunch can be done both internally, from the background plasma electrons, or externally, using an external particle source. External injection is of particular interest for reaching high beam energies, for example in linear particle collider applications [4,5], as this is related to so-called staging [6], i.e. concatenation of consecutive acceleration stages. Internal injection has the potential of generating ultra-high brightness beams because of the rapid acceleration and strong transverse focusing, which mitigate the impact of space-charge forces [7–13]. The injected particles can potentially also reach higher energies than the drive beam.

However, to properly utilize the strong accelerating fields in the wake without spoiling the beam quality, care must be taken when tuning the witness bunch parameters for the wake. Tailoring the

* Corresponding author.
E-mail addresses: jonas.bjorklund-svensson@desy.de (J. Björklund Svensson), sara.thorin@maxiv.lu.se (S. Thorin), olle.lundh@fysik.lth.se (O. Lundh).

https://doi.org/10.1016/j.nima.2022.166591
Received 21 December 2021; Received in revised form 4 March 2022; Accepted 9 March 2022
Available online 16 March 2022

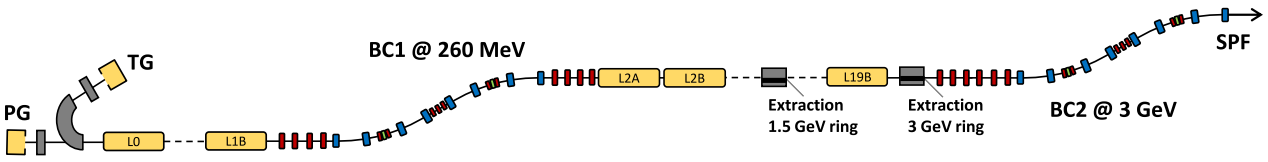

Fig. 1. Compact schematic layout of the MAX IV linac. Yellow denotes radio-frequency (RF) structures (also marked with L), quadrupole magnets are shown in red, dipole magnets in blue, sextupole magnets in green and special magnets in gray. PG and TG refers to the photocathode and thermionic RF guns, and BC1/2 to the first/second bunch compressor, respectively. A schematic of the SPF is shown in Fig. 2.

current profile of the witness bunch correctly with respect to the wake, i.e. beam-loading the wake, can minimize the induced correlated energy spread and increase efficiency [14,15], while matching the transverse beam size to the strong focusing inside the wake help mitigate betatron dephasing and potential emittance growth. Reaching these small matched β functions can be assisted by tailoring the density ramps at the entrance and exit of the plasma [16–19]. Such ramps can also serve to mitigate the hosing instability [20–22] triggered by transverse tilts along the bunches produced by, for example, coherent synchrotron radiation (CSR) [23] in bunch compressors or transfer lines.

Creating driver–witness bunch pairs externally can be done in different ways. One possibility, which has been experimentally demonstrated [15,24] at FACET [25] and FLASHForward [26], uses a dispersive collimation section with a mask or scraper to effectively remove the longitudinal center of a single bunch, which produces two distinct bunches after the dispersion is cancelled. While highly precise [27], such a solution is typically a large addition to experimental complexity and cost if implemented as an additional section of the accelerator layout. The dispersive elements can also introduce unwanted nonlinear effects in the beam through for example CSR. If the facility layout allows for it, the scraper could be placed inside a bunch compressor instead, similar to what has been done for free-electron laser (FEL) use at LCLS [28], reducing the overall complexity.

Another solution is to generate the driver–witness pairs directly in a photocathode electron gun (PG) by tailoring the laser pulses, as done, for example, in Refs. [29–31]. This must generally be done such that the bunches can be generated, accelerated, compressed, and focused together all the way through the accelerator. Such a scheme comes with its own set of difficulties, for example with space charge in the gun potentially causing bunch merging. However, producing both the driver and witness bunches in this way can provide an additional layer of control, and requires much less (or no) bunch charge to be collimated. It is also a relatively inexpensive way of generating multiple bunches as typically only a small modification of or addition to the gun laser system is required. Because of these advantages, this is the method that we choose for further study in this work, in the context of the MAX IV Linear Accelerator.

Previous work has strongly indicated that the MAX IV Linear Accelerator (linac) would be suitable for generating PWFA-appropriate beams [31,32]. In this study, start-to-end simulations of the PG, linac and beam–plasma interaction are used to further show the potential of the MAX IV linac as a driver of a PWFA experiment. To briefly summarize the results, this set of simulations show that it is viable to use the linac for PWFA applications with both single and double bunches. The single-bunch simulations show injection and acceleration of a 22 pC (1 kA) bunch from the background plasma to above 3 GeV, and the double-bunch simulations show an energy gain of 1 GeV (33%) of the witness bunch. The findings also motivate further investigations into this application. This study is also, to the authors' knowledge, the first comprehensive numerical study of a PWFA being driven by a linac with bunch compressors of the double-achromat type, giving valuable insight into the applications for such bunch compressors.

The article is laid out as follows. The MAX IV facility and Linear Accelerator are outlined in Section 2. The two main PWFA operation modes are described in Sections 3.1 and 3.2, which detail the individual simulations of the PG, linac and beam–plasma interaction separately. Appendices A and B provide more background on the features of the accelerator and optimizations of the linac lattice, respectively.

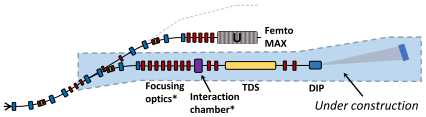

Fig. 2. Schematic of the SPF, with the 3 possible beamlines, of which FemtoMAX is the only populated to date. U denotes undulator. Color conventions are the same as for Fig. 1. Labels marked with asterisks (*) are proposed for the PWFA experiment. The blue field marks the section which is currently under construction.

2. The MAX IV Linear Accelerator

The MAX IV Linear Accelerator [33] is a warm, S-band electron accelerator, which serves as full-energy injector for the 1.5 and 3.0 GeV storage rings [34] as well as the Short-Pulse Facility (SPF) [35], which is located downstream of the injection point for the 3 GeV ring. A conceptual design report on using the linac as a driver for a soft X-ray FEL, named the SXL [36,37], was published in early 2021 [38]. A compact overview of the linac is shown in Fig. 1.

The starting point of the linac is one of two electron sources; one thermionic electron gun (TG) used for ring injection, and one PG used mainly for SPF delivery [39]. The PG is a warm copper gun with a copper cathode. Together with an emittance-compensating solenoid magnet and the first linear accelerating structure, the guns make up the pre-injector. The laser pulses driving the photoinjector [40] are stretched to nominally 3–6 ps FWHM quasi flat-top using a step-less 4-f UV pulse shaper [41]. The 39 linear accelerating structures are, like the gun, warm, S-band copper units.

For delivery to the SPF, the bunches are compressed longitudinally to yield shorter bunches with higher current than what is used for ring injection. In the MAX IV linac, this is done using dogleg-shaped double-achromat bunch compressors [42], which differ from the more commonly used chicane compressors in a few key ways. Unlike chicanes, the achromats have a positive first-order longitudinal dispersion, R_{56}, which means that a positive chirp, with respect to longitudinal bunch coordinate in the co-moving frame, ξ, is required for compression. This is achieved with a positive off-crest phase in the RF voltage. The naturally positive second-order longitudinal dispersion, T_{566}, is optimized with sextupoles in such a way as to cancel out the second-order longitudinal phase-space (LPS) curvature imposed by the RF voltage. This means that the LPS linearization is done using the optics alone — no higher-harmonic linearizing cavity is required. This compressor scheme is simple, reliable, and economical.

The nominal post-BC2 bunch parameters for SPF delivery are a duration of 100 fs, an emittance of <1mm mrad and a charge of 100 pC, with the purpose of creating spontaneous short-pulse X-ray undulator radiation. Previous simulations indicate that it is possible to compress the bunches to well below 100 fs FWHM and keep the emittance low [37,42]. The building layout of the SPF is such that there are three parallel slots to which the linac can supply the electron beam, see Fig. 2. To date, the only populated slot houses the FemtoMAX beamline [43].

2.1. Opportunities for PWFA

Currently, a diagnostics beamline is under construction in the SPF. Since its inception we have considered allocating space for a multi-purpose interaction chamber and a final focusing (FF) system in the same beamline, within an experiment we call PlasMAX. A schematic of the current design plan of the PWFA project is also shown in Fig. 2. In order to explore synergies between the projects and use the accelerator as efficiently as possible, the interaction chamber can be placed just upstream of the polarizable transverse deflecting structure (TDS) [44]. The FF magnets, see B, can then also be used to aid in matching the beam to the TDS optics. This layout should enable state-of-the-art diagnostics for the PWFA beam, similar to those at FLASHForward [45,46], while not interfering with regular linac diagnostics operation.

Another useful feature of the facility is that it is possible to enter the SPF hall while operating the linac for ring injection; if the beam is dumped at BC2 there is no radiation hazard in the SPF hall, which allows for work to be done inside the hall on a regular basis. This is a big advantage compared to other experiments on a similar scale, as larger work tasks on the experimental setups can typically only be performed a few times per year. Moreover, the area above the SPF hall houses space reserved for laser laboratories, enabling use of lasers for various applications (discussed further in Section 4).

Phase 1 of the beamline construction is being completed, and is focused on diagnosing ultra-short, high-brightness bunches. The proposed phase 2 introduces the final focus (FF), interaction chamber and capture optics. More details about this beamline and project can be found in Ref. [31].

3. Acceleration modes

Initially, two different operating modes are envisioned within the PWFA experiment; the first mode uses a single driver bunch to drive a "plasma cathode", where internal injection (based on, for example, density down-ramp injection [11,13] and plasma photocathode injection [7,12]) will be used to generate the witness bunch inside the plasma. The second mode operates as a "plasma booster" with two bunches in an external injection, driver–witness configuration. Each comes with its own set of difficulties; the simulations shown in this paper should serve as baseline examples of each mode. We denote the single-bunch, internal injection mode by P-1 and the double-bunch, external injection mode by P-2. In the P-2 mode, the main approach is to create the bunches in the PG by tailored laser pulses, but another possibility could be to also upgrade BC2 with a collimation system to create or manipulate the bunches there as well.

3.1. Plasma cathode with single bunches: P-1

3.1.1. Photocathode gun

The first section of the accelerator is the PG, followed by a solenoid used for emittance compensation, and a linac section used to boost the energy to approximately 100 MeV where the space charge forces become negligible. The code `ASTRA` [47] is used to simulate this section of the machine, and the number of slices and time steps were chosen to obtain stable results while properly resolving the processes in the short beam. In order to resolve features of the individual bunch slices, 10^6 particles are used.

A bunch with 200 pC charge is generated from an initial laser pulse with a truncated Gaussian transverse distribution [48] and a Gaussian-like longitudinal distribution. The transverse RMS size of the pulse is 0.4 mm and the initial duration is short, 100 fs RMS, in order to produce a short bunch out from the first linac. The gun electric field is set to 120 MV/m, and the bunch is injected at 30 degrees with respect to zero-crossing. Due to the short initial length of the bunch, it expands close to the blowout regime in photoinjectors [49,50] (not to be confused with the blowout regime in the plasma) where strong space charge forces are present. Using small time steps, the injector parameters were optimized with an emphasis on keeping the bunch relatively short and with a maximum normalized emittance of approximately 0.8 mm mrad.

While this operating point could provide challenging to use because of the short laser pulse duration, preliminary simulations indicate that similar bunch parameters at the end of the pre-injector can be reached with different sets of initial pulse and bunch parameters. However, more detailed simulations would be needed to determine which, if any, of the possible limitations are reached during the beam setup. The bunch parameters after the pre-injector are shown in Fig. 3(a) and (b) and Table 1.

3.1.2. Linac

The simulations of acceleration, compression and final focusing in the linac are done using the particle tracking code `Elegant` [51].

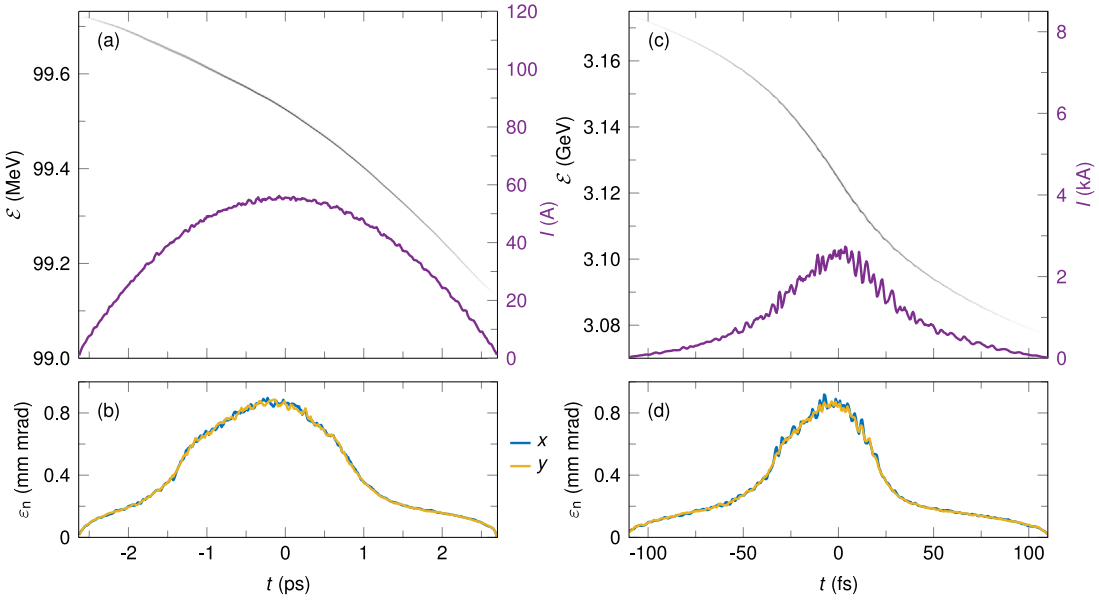

Fig. 3. Longitudinal ($t - \mathcal{E}$) phase space of beam after the injector (a) and at the focal plane (c), shown in grayscale. Darker shade means higher particle density. The overlaid purple curve depicts the beam current profile. (b), (d) Slice normalized emittances at the respective locations, with blue for x and yellow for y.

Table 1
Summary of the injector and linac simulation results for P-1. The given values are the projected values within 1.5 times the temporal FWHM, τ. The values are given at two locations along the simulation: after the injector and at the focal plane.

P-1	$\langle\mathcal{E}_b\rangle$ MeV	σ_δ % RMS	$\epsilon_{n,x}/\epsilon_{n,y}$ μm	σ_x/σ_y μm RMS	β_x/β_y cm	τ fs FWHM	I_p A	n_b 10^{17} cm^{-3}	Δx μm
Injector	99.5	0.13	0.55/0.55	105/108	389/391	3740	56	0.3e−3	0.3 ± 0.8
Focal plane	3120	0.48	0.69/0.66	4.2/4.2	15.9/15.9	53	2740	5	1.6 ± 1.0

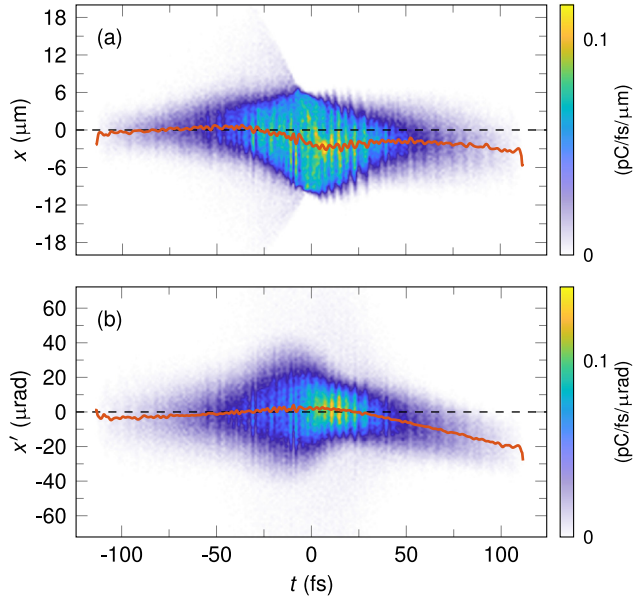

Fig. 4. $t-x$ (a) and $t-x'$ (b) phase space densities of the beam at the focal plane, shown in blue–yellow color scale. The overlaid red curve depicts the beam slice centroids obtained from a Gaussian fit to each slice. The axis scaling in (a) is chosen such that it shows the true physical aspect ratio of the beam.

The tracking in `Elegant` is fed by the `ASTRA` simulation output and thus starts after the pre-injector, at 100 MeV, and ends at the FF focal plane, at 3 GeV. The linac and FF optimizations are described further in Appendix B. Both wakefields and (1D) CSR are enabled. The systematic multipole content used for the magnets come from typical measurements of the installed magnets.

The beam parameters at the focal plane are shown in Fig. 3(c) and (d) and Table 1. The bunch duration is $\tau = 53$ fs FWHM, yielding a peak current of $I_p = 2.74$ kA. Together with the focal spot RMS radii of $\sigma_x = 4.4$ μm and $\sigma_y = 4.5$ μm at $t = 0$, the peak bunch electron density is $n_b \gtrsim 5 \times 10^{17}$ cm^{-3}. The bunch duration, together with the bunch electron density, makes a plasma density of $n_p = 1 \times 10^{17}$ cm^{-3} appropriate for the subsequent plasma stage, as the bunch length is then slightly shorter than half the linear plasma wavelength and $n_b \gtrsim 5 \times n_p$. Based on the slice normalized emittance of $\epsilon_n \approx 0.8$ mm mrad around $t = 0$ (see Fig. 3(d)), the β function is set to a shallow 15 cm. This is substantially larger than the matched β function of approximately 1.8 mm at the given electron energy and plasma density, but the difference between vacuum and plasma β functions can be bridged using, for example, a long, adiabatic density ramp [16–19].

Fig. 4 shows a projection of the beam in $t - x$ and $t - x'$ space at the focal plane, where small CSR-induced beam tilts can be seen. These modest tilts are achieved by the method used in Ref. [52], where the transverse dispersions in BC2 are de-tuned to straighten the bunch. Unlike the case in Ref. [52], the tilts observed here are predominantly of second order, wherefore tuning with the bunch compressor sextupoles is the preferred strategy. The linear component of the tilt is mitigated by a slight detuning of the quadrupoles in the second BC2 achromat, to give a non-zero first-order transverse spatial and angular lattice dispersion, R_{16} and R_{26}, respectively. This also alters the longitudinal dispersion, R_{56}, slightly and requires a small shift in the accelerating phase in the main linac to regain the desired bunch length after BC2. The second-order dispersions are tuned to 3.2×10^{-3} m, 8.5×10^{-3} m and 4.0×10^{-2} m for T_{166}, T_{266} and T_{566}, respectively.

From Fig. 4, it is evident that the beam tilts could not presently be completely cancelled. The maximum spatial offset for an individual slice inside $t = \pm 50$ fs is 3.3 μm, and the RMS size of that slice is 4.3 μm, while the RMS size at $t = 0$ is 5.4 μm according to a Gaussian fit. It is, however, clear that in x, the beam distribution near $t = 0$ is no longer Gaussian, but exhibits a shape which is more flat-top. Regardless, the tilts are relatively small compared to the beam size, which should increase stability in the plasma [22]. No tilts are observed in the y-direction.

3.1.3. Beam–plasma interaction

The interaction between the beam driver and the plasma is simulated using the particle-in-cell (PIC) code `CALDER` [53,54] in a 3D geometry in order to properly model asymmetric effects and wave-breaking. Because of the bunch parameters described above, a plasma density of $n_p = 1 \times 10^{17}$ cm^{-3} is used. We consider a fully-ionized plasma consisting of a linear density ramp from 0 to n_p followed by a density plateau (see Fig. 5(a)). A moving window of 240 × 162 × 162 cells follows the electron beam, with longitudinal and transverse steps $\Delta\xi = \Delta x = \Delta y = 0.75$ μm. The time step is $\Delta t = 1.45$ fs. One macro-particle per cell is used for the cold electrons of the plasma, while the electron beam is initialized from a file containing 2.5×10^5 equally weighted particles sampling the `Elegant` results from Section 3.1.2 above. The plasma ions are considered immobile.

The start of the density up-ramp is placed at the vacuum focal plane. A linear ramp is used as adiabatic density up-ramps are harder to simulate accurately. A cross-section of the beam–plasma interaction and the corresponding on-axis longitudinal electric field at the start of the density plateau are shown in Fig. 5(c). The oscillation of the bunch tail is caused by the incoming spatial and angular transverse bunch tilts visible in Fig. 4. With these bunch and plasma parameters, an accelerating field reaching a maximum of 20 GV/m at the end of the first wake period is generated.

The evolution of the on-axis longitudinal electric field, E_ξ, during the propagation in the plasma is shown in Fig. 5(b), and exhibits excellent stability for nearly the whole range of the simulation, up to almost half a meter. Towards the end of the simulation, perturbations start to appear, as the driver energy, W_b, has depleted to below 30% of its initial value at this point (see black curve in Fig. 5(a)). Even if the driver still contains a substantial amount of energy, the energy loss is unequally distributed over the current profile because of the profile of the accelerating field, see Fig. 5(c). E_ξ locally peaks at about $\xi = x - ct = 0$, near the middle of the driver beam, and the electrons located at this position have lost their entire energy and thus dephase in the wakefield which degrades the accelerating structure. This uneven deceleration can be mitigated by tuning the bunch current profile into an asymmetric up-ramp, which can also increase the transformer ratio (i.e., the ratio between decelerating driver field and accelerating witness field) [55–57]. Such bunch current tuning was previously demonstrated experimentally at the MAX IV linac [31].

In order to evaluate the possibility of acceleration in this structure, the density profile is modified by adding a short density spike with a Gaussian profile, characterized by a peak of $n_p = 1 \times 10^{18}$ cm^{-3} and RMS width $\sigma_{n_p} = 75$ μm centered at $s = 15$ cm (see Fig. 6(a)). The

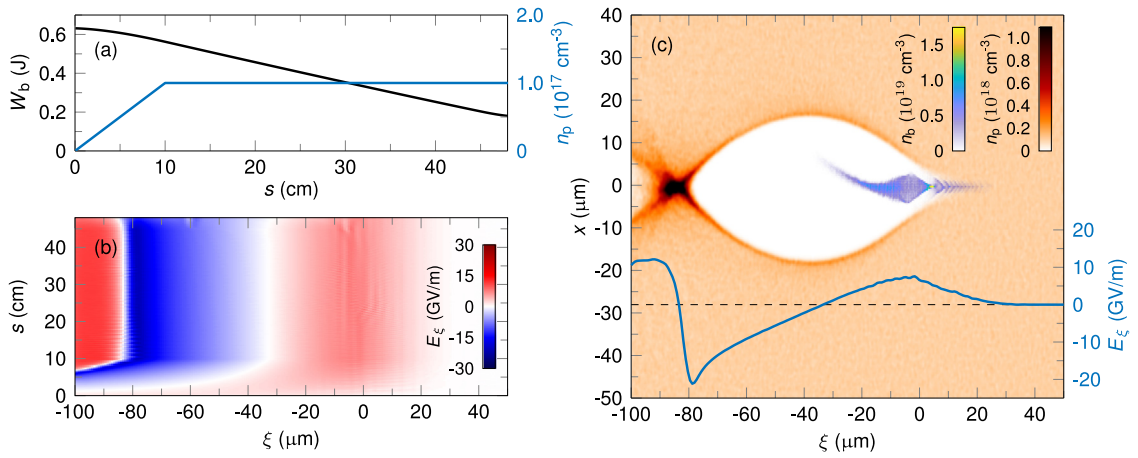

Fig. 5. (a) Density profile for the plasma (blue) and total energy of the driver (black) as a function of the propagation distance s. (b) Longitudinal electric field E_ξ on the propagation axis as a function of s. $\xi = s - ct$ is the longitudinal coordinate in the co-moving frame. (c) Density plot of the $x-\xi$ space inside the plasma, at the start of the plateau at $s = 10$ cm. The plasma electron density n_p, is represented in red-black scale, and the beam electron density, n_b, in blue–green-yellow. The blue curve shows the longitudinal electric field E_ξ on the propagation axis.

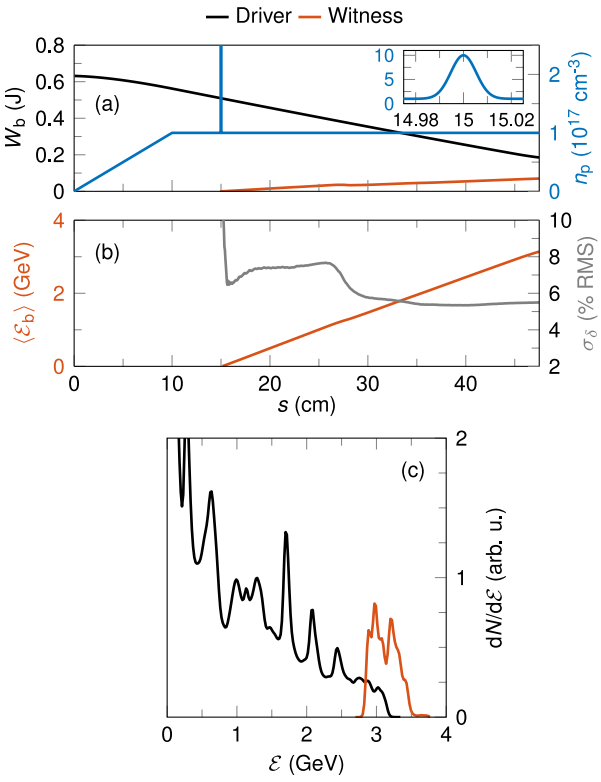

Fig. 6. (a) Total energy of the driver (black) and the injected/witness bunch (red) as they propagate through the plasma density profile shown in blue. (b) Evolution of the mean witness electron energy (red) and RMS relative energy spread (gray). (c) Spectra of the driver (black) and injected bunch (red) at the simulation end.

density spike triggers injection in the down-ramp [11] of a 30 pC (of which 22 pC survives), 22 fs FWHM (1 kA) bunch which reaches a final mean energy of approximately 3.15 GeV. The total energy of the injected witness bunch is visualized in Fig. 6(a) (red). After 48 cm, the energy of the witness bunch reaches 70 mJ. This yields a total energy transfer efficiency of about 11% from the initial energy contained in the driver. When considering the total energy of the driver at $s = 15$ cm, the efficiency of the energy transfer climbs to 14%. The efficiency is limited by the charge ejection occurring at the rear of the witness bunch between $s = 25$ cm and $s = 30$ cm, as well as the beam loading not being optimal [14] and the driver being unevenly decelerated. Note that the total energy of the driver beam (black curve in Fig. 6(a)) is similar to the one in Fig. 5(a), meaning that the presence of the density spike does not significantly affect the driver. The instantaneous energy transfer in each time step climbs to 23%.

In Fig. 6(b), the mean electron energy of the witness (red) shows stable gain at approximately 10 GeV/m. This is lower than the maximum value observed in Fig. 5(b) and (c) as the witness is not injected exactly at the extreme rear of the bubble, and that it partially loads the wake which decreases the maximum electric field strength. The RMS energy spread stabilizes at about 5.5% (gray curve), due to the variation of E_ξ over the length of the bunch. Fig. 6(c) shows the final spectra of the driver and witness bunches.

These simulations show that the stability of the accelerating field shown in Fig. 5(b) can be used to transfer energy to an internally injected witness beam. The modest energy transfer efficiency and large energy spread is partially due to the wake being far from optimally beam-loaded, which could be improved for example by tailoring of the density spike used for the down-ramp injection and the driver current profile. An optimized driver current profile could also increase the total effective acceleration length and transformer ratio, thereby increasing the total efficiency further. The results also highlight that in spite of some tilts in the driving beam, a bunch can be injected and accelerated over many tens of betatron wavelengths.

3.2. Plasma booster with double bunches: P-2

3.2.1. Photocathode gun

The machine layout for the double-bunch simulations is the same as for the P-1 mode (Section 3.1.1). The difference is that a double-bunch beam with 120 pC in the driver and 80 pC in the witness bunch is used, and the number of macroparticles is 2×10^6. The driver bunch is emitted first in time and experiences a lower field in the gun, and space charge effects on the beam will be more pronounced due to this lower field. However, the requirements on the driver bunch can be slightly relaxed compared to those on the witness. The witness bunch, emitted a few ps after the driver bunch, will also see a lower field gradient due to the shielding from the driver bunch, which can degrade the beam quality of the witness bunch. Ref. [58] provides more details on the pre-injector simulations for the double-bunch scenario. The working point is found by operating as close as possible to an emittance compensated beam for the witness bunch, while keeping acceptable parameters on the driver bunch.

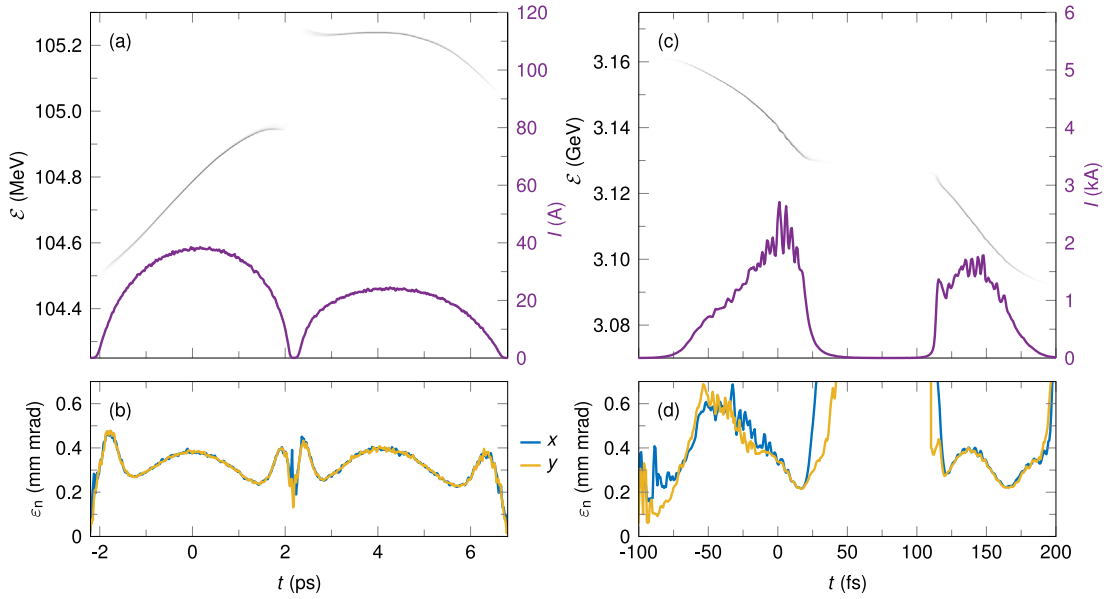

Fig. 7. Longitudinal ($t-\mathcal{E}$) phase space of beam after the injector (a) and at the focal plane (c), shown in grayscale. Darker shade means higher particle density. The overlaid purple curve depicts the beam current profile. (b), (d) Slice normalized emittances at the respective locations, with blue for x and yellow for y.

The best results from the simulations, with a realistic maximum field in the PG of 120 MV/m, is found when the center of the double-bunch structure is injected at 40 degrees phase from zero crossing. The transverse RMS sizes for the driver/witness are 0.65/0.60 mm with a cut-Gaussian like transverse distribution where the parameters of the transverse shape have been optimized for the best emittance. Both bunches have the same longitudinal profile, which is a top-hat like distribution with a FWHM of 2.4 ps and rise/fall times of 1 ps. The separation between the two bunches is 4.6 ps center-to-center and the ASTRA simulation results for the double-bunch beam are shown in Fig. 7(a) and (b) and Table 2.

3.2.2. Linac

Particle tracking through the linac was done with similar settings to the P-1 tracking (Section 3.1.2), with a few adjustments to the accelerating phases and optics to better accommodate the double-bunch beam. The bunch parameters at the focal plane are shown in Figs. 7(c) and (d), 8 and Table 2. As shown in Fig. 7(c), the driver bunch current profile is now an up-ramp as a result of the off-energy LPS linearization, while the witness bunch is more linearized. Because of the relatively hard compression, the bunch separation centroid-to-centroid is 147 fs and the driver bunch peak current is 2.3 kA. However, due to the low and maintained (around the current peak) slice emittance (c.f. Fig. 7(b) and 7(d)), the driver bunch electron density again reaches roughly 5×10^{17} cm^{-3}. This bunch density makes also this beam suitable for a plasma of density 1×10^{17} cm^{-3}, although the linear plasma wavelength of 105 μm $\leftrightarrow$ 350 fs is a bit longer than the full beam.

The relatively large full-beam energy spread (2.2% end-to-end) causes some chromatic aberrations over the beam. Because the BC2 and FF optics were set with the witness bunch energy as nominal, the driver beam is slightly elliptic at the focal plane, although convergent because of its higher energy. These aberrations come, to a large extent, from around BC1, and removing them altogether is a difficult task because of the high energy spread throughout the whole accelerator.

The method used for P-1 for mitigating the beam tilts, by de-tuning the higher-order transverse dispersion in BC2, does not work as well for a double-bunch structure; since the higher-order dispersion tuning relies on a certain working point in energy, it can only effectively be used on one bunch at a time. Nevertheless, some tilt compensation was done with the energy centered on the witness bunch, partially reducing the variation in spatial offsets while introducing a small amount of near-constant angular offset for both bunches. The tilts shown in Fig. 8 are a combination of leaking higher-order dispersion from BC1 and CSR from BC2 after mitigation was done. The offset difference between the bunch centroids, $\Delta x_{\mathrm{D-W}}$, is small (see Table 2 and Fig. 8(a)), although there are clear tilts within each bunch on the order of the bunch size. The angular offset between the bunches, see Fig. 8(b), is negligible compared to the angular tilt within the driver bunch.

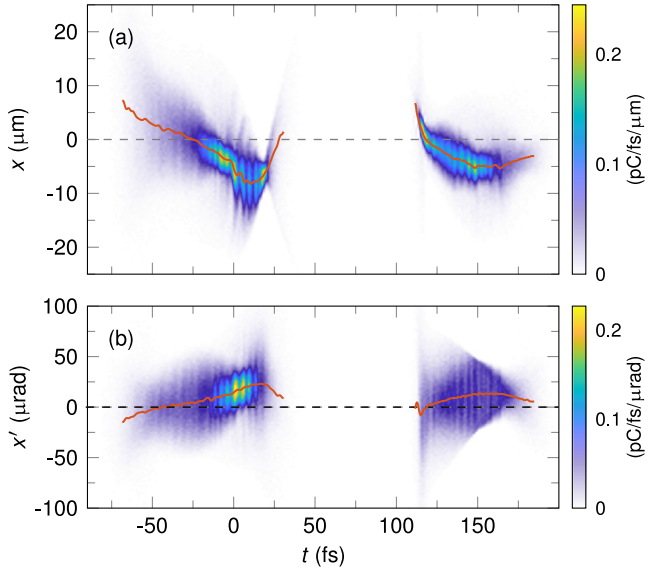

Fig. 8. $t-x$ (a) and $t-x'$ (b) phase space densities of the beam at the focal plane, shown in blue–yellow color scale. The overlaid red curve depicts the beam slice centroids obtained from a Gaussian fit to each slice. The axis scaling in (a) is chosen such that it shows the true physical aspect ratio of the beam.

3.2.3. Beam–plasma interaction

PIC simulations are carried out in a similar manner to the P-1 mode (Section 3.1.3), with a 10 cm long linear density up-ramp followed by a plateau at $n_p = 1\times10^{17}$ cm^{-3} (see Fig. 9(a)). The electron bunches are now initialized from 2.5×10^5 particles sampling the Elegant

Table 2
Summary of the injector and linac simulation results for P-2. The given values are the projected values within 1.5 times the temporal FWHM, τ. The values are given at two locations along the simulation: after the injector and at the focal plane. Δx and $\Delta x_{\mathrm{D-W}}$ denote the absolute median ± RMS slice spatial centroid offsets within and between bunches, respectively.

P-2		$\langle\mathcal{E}_b\rangle$ MeV	σ_δ % RMS	$\epsilon_{n,x}/\epsilon_{n,y}$ μm	σ_x/σ_y μm RMS	β_x/β_y cm	τ fs FWHM	Δt fs	I_p A	n_b 10^{17} cm^{-3}	Δx μm	$\Delta x_{\mathrm{D-W}}$ μm
Injector	D	104.8	0.12	0.58/0.58	65.9/65.8	155/154	3420		39	1.3e−3	0.3 ± 0.6	
	W	105.2	0.04	0.55/0.54	74.9/74.5	211/210	3570	4100	25	0.4e−3	0.6 ± 0.8	0.3 ± 1.0
FF	D	3141	0.19	0.62/0.46	5.27/2.57	27.6/8.9	46		2300	5	−3.4 ± 2.7	
	W	3110	0.27	0.56/0.54	3.8/3.2	15.5/11.5	55	147	1700	6	−3.7 ± 2.4	−0.3 ± 3.4

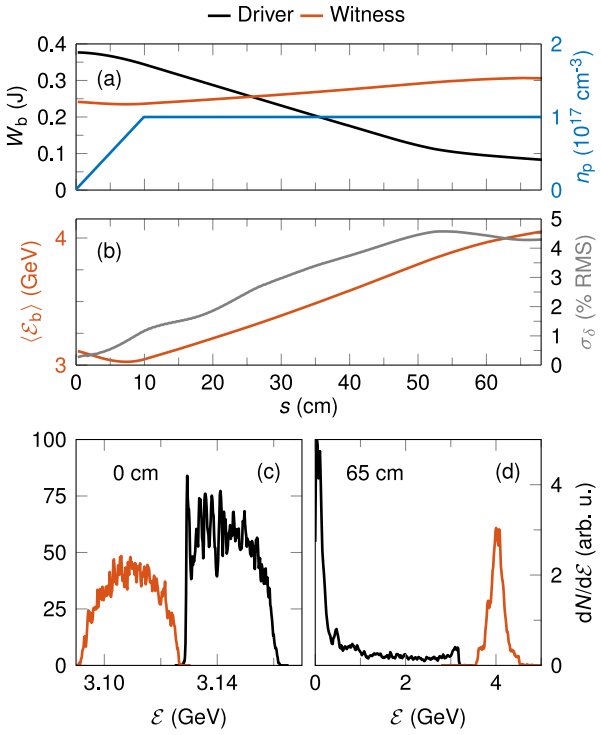

Fig. 9. (a) Total energy of the driver (black) and witness (red) as they propagate through the plasma density profile shown in blue. (b) Evolution of the mean witness energy (red) and RMS energy spread (gray). (c) Initial and (d) final energy spectra of the driver (black) and witness (red).

results from the previous section. Other parameters are kept identical to Section 3.1.3.

Fig. 9(a) shows a net energy transfer from the driver to the witness, although also the witness initially loses energy in the density ramp since it is located in the decelerating front of the bubble when the density is low. However, once inside the density plateau, the witness starts gaining energy, while the driver gets nearly entirely depleted after 65 cm of propagation. The total energy transfer efficiency from the driver to the witness is 18% after the whole simulation length. The instantaneous efficiency reaches 28% in the density plateau, which indicates that the total efficiency should be improved with shorter or nonlinear ramp profiles [16–19] because of decreased initial deceleration. The charge transmission to the end of the simulation is 98%, with most of the loss occurring towards the end of the simulation where the driver has lost too much energy to maintain the wake structure.

Fig. 9(b) shows gain of the mean witness electron energy at a rate of about 2 GeV/m inside the plateau, ending at 4 GeV after a gain of nearly 1 GeV, but the energy spread also increases to just above 4% RMS because of insufficient beam-loading. Both maximum and sampled accelerating field is consistently lower here than in the P-1 scenario; this is expected from a lower-current driver [3] and a larger degree of beam-loading [14], as well as the witness occupying an earlier phase in the bubble.

The initial and final energy spectra for both bunches are shown in Fig. 9(c) and 9(d), respectively. While the increase in energy spread is evidence that the witness has not fully loaded the wake, the large fraction of low-energy electrons in the driver (see Fig. 9(d)) is a clear signature of a more advantageous driver current profile than in the P-1 results (c.f. Fig. 6(c)). The driver current up-ramp here helps to flatten the decelerating wakefield, making the driver electrons lose energy at nearly the same rate and thus help extend the effective acceleration distance while also increasing the potential transformer ratio. This works towards increasing the efficiency compared to the case shown in Section 3.1.3, although there is still some room for improvement.

Finally, we note that the simulations show successful acceleration over long distances in spite of the beam tilts seen in Fig. 8(a) and (b). This is in part thanks to the witness occupying a relatively early phase of the wake where the bubble size is larger, which trades accelerating gradient for stability since some transverse oscillations of the bunch occur. It is also worth mentioning that the witness emittance does increase because of the transverse mismatch between the in-vacuum and in-plasma beam parameters which are not properly bridged by the linear density ramp. Nevertheless, these simulations demonstrate that the MAX IV linac can be used for PWFA acceleration in the two-bunch configuration. While we have here focused more on the longitudinal properties, further studies could optimize the focal parameters and vacuum plasma boundaries to improve the transverse emittance and energy gain of the witness beam.

4. Summary and outlook

To summarize, we have investigated the feasibility of using the MAX IV Linear Accelerator as a driver for beam-driven plasma-wakefield applications using numerical start-to-end simulations. The general conclusion of this study is that such an application is feasible, particularly if additional magnets can be installed to reduce the chromaticity and increase the flexibility of the linac optics (see Appendix B). The proposed modifications would be beneficial for linac performance in general, and are aligned with those implemented in the SXL CDR [38].

Two operating modes were studied: a single-bunch mode for internal injection (P-1) and a double-bunch mode for external injection (P-2). Both modes largely achieved their goals: the P-1 bunch was used to inject a 22-pC (1-kA) bunch in the plasma and accelerate it to over 3 GeV, and the P-2 beams were used to boost the witness particle energy by 1 GeV (33%). The simulations also highlighted that in spite of some residual tilts being present in the bunches, and the PWFA scheme generally being sensitive to such beam tilts, no hosing instability developed although transverse bunch centroid oscillations were observed. The growth of these oscillations occurred to the largest extent in the linear plasma density up-ramp. No charge loss from such oscillations occurred in the P-2 simulations because of the witness bunch being located further forward in the wake compared to the internally injected bunch in P-1.

To produce a PWFA-optimized bunch, minimizing beam tilts is paramount; to this end, work on further reducing CSR kicks in dogleg-shaped achromat-based bunch compressor systems is the subject of future investigations. However, it is worth noting that the 1D CSR

model in `Elegant` has been shown to overestimate the CSR-induced emittance growth for bunches of similar duration and current compared to 3D codes and experiment [59,60]. This reflects well on the presented results, as the beam tilts could in reality be smaller than those observed here; any future studies will also include more realistic CSR models.

Employing passive methods for minimizing transverse centroid oscillations in the plasma is nevertheless a reasonable complement to straightening the beam coming from the accelerator. One method could be using a higher-emittance driver bunch [22], for example by increasing its charge density in the PG, but it is not trivial to create such a diverse double-bunch structure in the PG which can be transported well to the focal plane, and it also puts additional demands on the gun and laser systems. Asymmetric current distributions between bunches also makes CSR compensation more difficult. Another way to further decrease the transverse oscillations is to employ adiabatic density ramps [21], which also facilitate matching the beam to the focusing forces inside the PWFA.

Generating and controlling entrance and exit plasma ramps is not trivial; an attempt to design a suitable plasma source was not made during this study and is left as the topic of future work. The two most common techniques for generating the main plasma column are through laser-ionizing vaporized alkali gases inside a heat-pipe oven [61–63] and through high-voltage discharge-ionizing room-temperature gases in capillaries [64]. Sharp density down-ramps for PWFA have hitherto been created by generating a second, perpendicular plasma column using a transversely propagating laser pulse which ionizes lower-lying electronic states of the employed gas species [12,13]. All of these techniques, and perhaps others, would be possible to use in the SPF hall because of the close access to laser laboratory and other auxiliary space.

In this study, the bunches were generated directly in the photocathode gun. As seen in Fig. 7(c), the optical phase space linearization mechanism employed here automatically skews the current profiles for the P-2 double-bunches in the direction of the most efficient wake excitation, transformer ratio and beam loading [14,55–57,65], without the use of collimators. The P-1 bunch current was kept symmetric in this study, but single bunches can be seamlessly tuned to yield nearly trapezoidal current profiles using this type of bunch compressor, as demonstrated experimentally in Ref. [31].

These observations indicate that achromat-based bunch compressors are useful for various wakefield-based schemes, and further study of such systems for these applications is warranted. For future studies, different ways of generating and/or tuning the bunch structures could be investigated to achieve more optimized results. For example, while the current profiles for P-2 were not completely optimal, see Figs. 7(c) and 9(d), it is likely that a spatially and temporally tuned laser profile (potentially together with a collimator in BC2, as in Ref. [28]), could lead to significantly improved results [66]. Even if parts of the beam are scraped off to optimize witness energy gain, beam loading, and charge coupling, the amount of charge which needs to be removed can be much less than purely scraper-based methods [15,24]. This serves to increase the overall efficiency of the scheme, and avoiding excessive collimation also makes the scheme suitable for high repetition rate applications.

Apart from that the double-achromat bunch compressors passively skew the current profiles of driver and witness in the respective appropriate directions, recent results show that bunch compressor systems with positive R_{56}, such as these, can also provide a passive stabilization of the beam energy with respect to RF modulator high-voltage jitter. More information about this can be found in Ref. [38] and will be further detailed in an upcoming publication. While the working point used in this study is not operating at the optimal RF phases (with respect to jitter stabilization), future work on similar systems should consider this as an optimization variable.

In conclusion, there are several advantages to building an experimental research chamber in the linac diagnostics beamline. There is no other linac that currently employs similar double-achromat bunch compressors, allowing for unique research opportunities in, for example, bunch current shaping for wake-based schemes. Furthermore, the attainable electron energies (3–4 GeV, and potentially higher) is in between other GeV-class PWFA experiments, such as FLASHForward (1–2 GeV) and FACET-II (>10 GeV), an energy range which is highly interesting for light-source applications. Apart from plasma-based wakefield experiments, experiments with wakefields in, for example, metallic and dielectric structures could be performed in the same interaction chamber, which could be interesting from the FEL perspective. The possibility of performing on-site experiments would therefore also bring unique opportunities for studies of various wakefield-based bunch manipulation schemes [67–69]. Space for the experimental chamber is already allocated in the diagnostics beamline, without interfering with regular operation, which facilitates a potential implementation from the infrastructure point of view. The possibility of safely blocking the beam to the SPF while allowing ring injection would allow for excellent accessibility to the interaction chamber area, which is rare for accelerator facilities. This project therefore enables a cost-effective implementation of a cross-disciplinary experimental platform with unique R&D opportunities for wake-based experiments aimed at PWFA and FEL.

CRediT authorship contribution statement

J. Björklund Svensson: Conceptualization, Methodology, Investigation, Writing – original draft, Writing – review & editing, Visualization, Project administration. **J. Andersson:** Investigation, Writing – original draft. **J. Ferri:** Investigation, Writing – original draft, Visualization. **T.K. Charles:** Writing – review & editing, Supervision. **H. Ekerfelt:** Conceptualization, Investigation. **E. Mansten:** Conceptualization, Writing – review & editing, Supervision, Project administration. **S. Thorin:** Conceptualization, Writing – review & editing, Supervision. **O. Lundh:** Conceptualization, Writing – review & editing, Supervision, Funding acquisition.

Declaration of competing interest

The authors declare that they have no known competing financial interests or personal relationships that could have appeared to influence the work reported in this paper.

Acknowledgments

The authors thank Michael Borland for extensive help and feedback regarding `Elegant`, and Filip Lindau and Marija Kotur for technical feedback and support concerning the MAX IV gun laser system. We also acknowledge the support of the Swedish Research Council (VR 2016–03329, 2019–04784), the Knut and Alice Wallenberg Foundation (KAW 2019.0318), and the European Research Council (ERC-2014-CoG 647121). Research conducted at MAX IV, a Swedish national user facility, is supported by the Swedish Research Council under contract 2018–07152, the Swedish Governmental Agency for Innovation Systems under contract 2018–04969, and Formas under contract 2019–02496.

Appendix A. Some features of the MAX IV linac BCs

Longitudinal RF wakefields in the linac structures influence the bunch chirp, and the effects of these wakefields increase with the bunch current [70]. Since the energy chirp is positive with respect to ξ, and the wakefields cause a progressive decrease in particle energy towards the back of the bunch, the wakefields chirp in the same direction as the RF voltage, which leads to a stronger compression. This was studied in Refs. [71,72] for single bunches in the MAX IV linac. Because of the current dependence on the wakefields, the bunch current after BC1

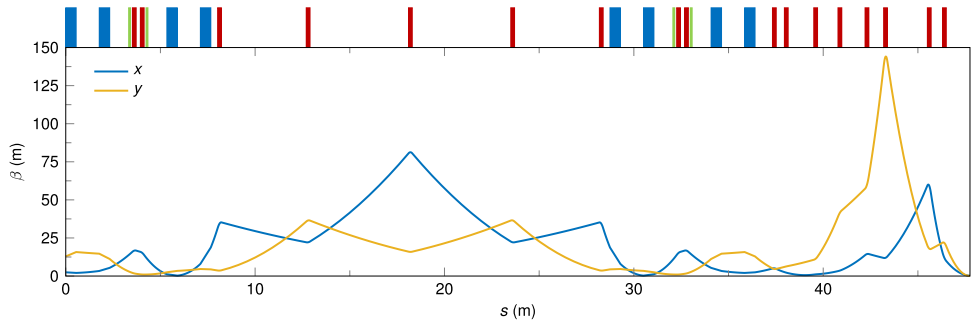

Fig. B.1. The magnet lattice and β functions of BC2 and the FF. Dipole magnets are blue, quadrupole magnets are red and sextupole magnets are green.

must be matched to the RF phase in the main linac for the desired compression in BC2. This also influences the LPS curvature, which BC2 must subsequently be tuned to linearize. The sign of the chirp also has the effect that dechirping the bunches using passive, wake-based techniques [67–69] is not possible, as such an operation would instead increase the chirp.

Another effect of the employed bunch compression scheme is that for the double-bunch mode, the driver bunch, which arrives closer to the peak of the RF voltage than the witness, will in many cases obtain a smaller (and less linear) chirp than the witness bunch, particularly in linac section L1, before BC1 (see Fig. 1). Because the linearization scheme is based around a working point in relative energy deviation at $\delta = (\mathcal{E}_b - \langle\mathcal{E}_b\rangle)/\langle\mathcal{E}_b\rangle = 0$, which is normally placed at the center of a single bunch, the linearization cannot be optimal for both bunches simultaneously. Therefore, the driver bunch can become under-linearized while the witness bunch becomes over-linearized, leading to an asymmetric current distribution within and between the bunches. This asymmetric compression also influences the wakefields in the main linac. However, this asymmetry in compression can also serve to produce ramped current profiles with opposite slopes [31], which are near-optimal shapes from a plasma-wake loading point of view [14,65].

Appendix B. Optimizations of the linac lattice

When creating the double-bunch structure in the PG, the combined compression in BC1 and BC2 is naturally responsible for the final bunch durations and separation. One can shift the compression factor from one compressor to the other to tune the bunch separation while keeping the bunch durations relatively constant, at the expense of altered energy spread. Since the compression is tuned by the accelerating RF phase and wakefields of the bunches, the energy spread of the beam is directly affected by such a manoeuvre. The double-bunch time structure is rather long after the injector, see Fig. 7(a), which causes such beams in particular to gain a large energy spread; for appropriate final beam parameters, the end-to-end energy spread can reach above 6% at BC1 and 2% at BC2. This can cause large deviations in both the slice Twiss functions and the slice centroids in transverse position and angle, both between and within the bunches, which then affects downstream transport, compression, and focusing.

To combat these effects, and thus accommodate beams with larger energy spread, an effort was made towards making the compressors higher-order achromatic and tuneable to mitigate CSR kicks [52], and some work was done towards reducing the chromaticity of the optics throughout the accelerator. Compared to the BC2 layout shown in Ref. [52], the layout used for these simulations has the octupoles removed to reduce complexity (at the expense of some third-order control), since the transverse dispersion is dominated by first- and second-order terms at typical energy spreads in BC2. As in Ref. [52], the footprint of the compressor is unchanged, simplifying a potential machine upgrade. Four additional quadrupoles were added to previously vacant locations in the main linac, to reduce the maximum β functions and decrease the chromaticity of the main linac optics. An additional family of sextupoles in each achromat and new quadrupoles in the center straight section of BC1 were also added, retaining the footprint and reducing the chromatic degradation of that compressor as well. The total upgrade of the magnet layout compared to the current state, omitting the FF, is then comprised of a relocation of 3 quadrupoles and 2 sextupoles, and an addition of a total of 15 magnets (5+4+2 quadrupoles and 2+2 sextupoles) in the whole machine.

The current version of the final focus system consists of 8 quadrupole magnets. The original version of the optics was designed such that they, from the entrance of the first dipole magnet in BC2 to the focal point, were quasi-apochromatic [73]. In this case, the first order energy derivatives of the β functions, $d\beta/d\delta$, had been cancelled at the focal plane, which could not be fully done for α. The two remaining degrees of freedom (apart from the transverse Twiss parameters and the energy derivative of β) were instead used to limit the maximum β function value through the FF optics. This was observed to have a substantial impact on the vertical chromaticity. However, in spite of efforts to minimize chromatic aberrations from around BC1, where the energy spread is the largest for both P-1 and P-2, some aberrations still occur. As the time slices of the beam begin to overlap during compression in BC2, the uncorrected aberrations from BC1 cause slice emittance growth, see Fig. 7(d). Therefore, the optics which are used for the double-bunch simulations, see Fig. B.1, are not apochromatic, as the presented layout is observed to reduce the overall final aberrations for P-2. While such a configuration cannot reverse the slice emittance growth, the beam Twiss parameters are transversely more uniform.

The second achromat in BC2 (see Fig. 2), together with the FF optics, are the only currently non-existing sections of the lattice (omitting the proposed linac additions above). The total length of the FF, from the end of BC2 to the focal plane, is 11.35 m, with a maximum quadrupole strength of $\kappa = 4.94\ \mathrm{m}^{-1} \Leftrightarrow g_q = 49.4$ T/m at 3 GeV. A gradient of 50 T/m is taken as a conservative upper bound for the magnets and could be relaxed by increasing the length of the corresponding quadrupoles, in particular the last two before the focal plane. The nominal β functions at the focus are around $\beta_x^* = \beta_y^* = 15$ cm. The BC2+FF lattice and β functions are shown in Fig. B.1. As only a few magnets are currently planned for the diagnostic beam line, there is still some flexibility with respect to the final length and layout of the FF and plasma chamber area, and the inclusion of for example active (discharge) [74,75] and/or passive [76] plasma lenses could be considered both up- and downstream of the main plasma cell.

References

[1] P. Chen, J.M. Dawson, R.W. Huff, T. Katsouleas, Acceleration of electrons by the interaction of a bunched electron beam with a plasma, Phys. Rev. Lett. 54 (1985) 693–696, http://dx.doi.org/10.1103/PhysRevLett.54.693, URL https://link.aps.org/doi/10.1103/PhysRevLett.54.693.

[2] R. Ruth, A. Chao, P. Morton, P. Wilson, A plasma wake field accelerator, Part. Accel. 17 (1985) 171–189, URL http://cds.cern.ch/record/157249/files/p171.pdf.

[3] W. Lu, C. Huang, M. Zhou, M. Tzoufras, F.S. Tsung, W.B. Mori, T. Katsouleas, A nonlinear theory for multidimensional relativistic plasma wave wakefields, Phys. Plasmas 13 (5) (2006) 056709, http://dx.doi.org/10.1063/1.2203364.

[4] T. Behnke, J.E. Brau, B. Foster, J. Fuster, M. Harrison, J. McEwan Paterson, M. Peskin, M. Stanitzki, N. Walker, H. Yamamoto, The International Linear Collider Technical Design Report, Tech. rep., CERN, 2013, URL https://ilchome.web.cern.ch/publications/ilc-technical-design-report.

[5] M. Aicheler, P. Burrows, M. Draper, T. Garvey, P. Lebrun, K. Peach, N. Phinney, H. Schmickler, D. Schulte, N. Toge, A Multi-TeV Linear Collider based on CLIC Technology: CLIC Conceptual Design Report, Tech. rep. CERN-2012-007, CERN, 2012, URL https://edms.cern.ch/document/1234244/7.

[6] C.A. Lindstrøm, Staging of plasma-wakefield accelerators, Phys. Rev. Accel. Beams 24 (2021) 014801, http://dx.doi.org/10.1103/PhysRevAccelBeams.24.014801, URL https://link.aps.org/doi/10.1103/PhysRevAccelBeams.24.014801.

[7] B. Hidding, G. Pretzler, J.B. Rosenzweig, T. Königstein, D. Schiller, D.L. Bruhwiler, Ultracold electron bunch generation via plasma photocathode emission and acceleration in a beam-driven plasma blowout, Phys. Rev. Lett. 108 (2012) 035001, http://dx.doi.org/10.1103/PhysRevLett.108.035001, URL https://link.aps.org/doi/10.1103/PhysRevLett.108.035001.

[8] F. Li, J.F. Hua, X.L. Xu, C.J. Zhang, L.X. Yan, Y.C. Du, W.H. Huang, H.B. Chen, C.X. Tang, W. Lu, C. Joshi, W.B. Mori, Y.Q. Gu, Generating high-brightness electron beams via ionization injection by transverse colliding lasers in a plasma-wakefield accelerator, Phys. Rev. Lett. 111 (2013) 015003, http://dx.doi.org/10.1103/PhysRevLett.111.015003, URL https://link.aps.org/doi/10.1103/PhysRevLett.111.015003.

[9] A. Martinez de la Ossa, J. Grebenyuk, T. Mehrling, L. Schaper, J. Osterhoff, High-quality electron beams from beam-driven plasma accelerators by wakefield-induced ionization injection, Phys. Rev. Lett. 111 (2013) 245003, http://dx.doi.org/10.1103/PhysRevLett.111.245003, URL https://link.aps.org/doi/10.1103/PhysRevLett.111.245003.

[10] G.G. Manahan, A.F. Habib, P. Scherkl, P. Delinikolas, A. Beaton, A. Knetsch, O. Karger, G. Wittig, T. Heinemann, Z.M. Sheng, J.R. Cary, D.L. Bruhwiler, J.B. Rosenzweig, B. Hidding, Single-stage plasma-based correlated energy spread compensation for ultrahigh 6D brightness electron beams, Nature Commun. 8 (1) (2017) 15705, http://dx.doi.org/10.1038/ncomms15705.

[11] A. Martinez de la Ossa, Z. Hu, M.J.V. Streeter, T.J. Mehrling, O. Kononenko, B. Sheeran, J. Osterhoff, Optimizing density down-ramp injection for beam-driven plasma wakefield accelerators, Phys. Rev. Accel. Beams 20 (2017) 091301, http://dx.doi.org/10.1103/PhysRevAccelBeams.20.091301, URL https://link.aps.org/doi/10.1103/PhysRevAccelBeams.20.091301.

[12] A. Deng, O.S. Karger, T. Heinemann, A. Knetsch, P. Scherkl, G.G. Manahan, A. Beaton, D. Ullmann, G. Wittig, A.F. Habib, Y. Xi, M.D. Litos, B.D. O'Shea, S. Gessner, C.I. Clarke, S.Z. Green, C.A. Lindstrøm, E. Adli, R. Zgadzaj, M.C. Downer, G. Andonian, A. Murokh, D.L. Bruhwiler, J.R. Cary, M.J. Hogan, V. Yakimenko, J.B. Rosenzweig, B. Hidding, Generation and acceleration of electron bunches from a plasma photocathode, Nat. Phys. 15 (11) (2019) 1156–1160, http://dx.doi.org/10.1038/s41567-019-0610-9.

[13] A. Knetsch, B. Sheeran, L. Boulton, P. Niknejadi, K. Põder, L. Schaper, M. Zeng, S. Bohlen, G. Boyle, T. Brümmer, J. Chappell, R. D'Arcy, S. Diederichs, B. Foster, M.J. Garland, P. Gonzalez Caminal, B. Hidding, V. Libov, C.A. Lindstrøm, A. Martinez de la Ossa, M. Meisel, T. Parikh, B. Schmidt, S. Schröder, G. Tauscher, S. Wesch, P. Winkler, J.C. Wood, J. Osterhoff, Stable witness-beam formation in a beam-driven plasma cathode, Phys. Rev. Accel. Beams 24 (2021) 101302, http://dx.doi.org/10.1103/PhysRevAccelBeams.24.101302, URL https://link.aps.org/doi/10.1103/PhysRevAccelBeams.24.101302.

[14] M. Tzoufras, W. Lu, F.S. Tsung, C. Huang, W.B. Mori, T. Katsouleas, J. Vieira, R.A. Fonseca, L.O. Silva, Beam loading in the nonlinear regime of plasma-based acceleration, Phys. Rev. Lett. 101 (2008) 145002, http://dx.doi.org/10.1103/PhysRevLett.101.145002, URL https://link.aps.org/doi/10.1103/PhysRevLett.101.145002.

[15] C.A. Lindstrøm, J.M. Garland, S. Schröder, L. Boulton, G. Boyle, J. Chappell, R. D'Arcy, P. Gonzalez, A. Knetsch, V. Libov, G. Loisch, A. Martinez de la Ossa, P. Niknejadi, K. Põder, L. Schaper, B. Schmidt, B. Sheeran, S. Wesch, J. Wood, J. Osterhoff, Energy-spread preservation and high efficiency in a plasma-wakefield accelerator, Phys. Rev. Lett. 126 (2021) 014801, http://dx.doi.org/10.1103/PhysRevLett.126.014801, URL https://link.aps.org/doi/10.1103/PhysRevLett.126.014801.

[16] K. Floettmann, Adiabatic matching section for plasma accelerated beams, Phys. Rev. ST Accel. Beams 17 (2014) 054402, http://dx.doi.org/10.1103/PhysRevSTAB.17.054402, URL https://link.aps.org/doi/10.1103/PhysRevSTAB.17.054402.

[17] X.L. Xu, J.F. Hua, Y.P. Wu, C.J. Zhang, F. Li, Y. Wan, C.-H. Pai, W. Lu, W. An, P. Yu, M.J. Hogan, C. Joshi, W.B. Mori, Physics of phase space matching for staging plasma and traditional accelerator components using longitudinally tailored plasma profiles, Phys. Rev. Lett. 116 (2016) 124801, http://dx.doi.org/10.1103/PhysRevLett.116.124801, URL https://link.aps.org/doi/10.1103/PhysRevLett.116.124801.

[18] R. Ariniello, C.E. Doss, K. Hunt-Stone, J.R. Cary, M.D. Litos, Transverse beam dynamics in a plasma density ramp, Phys. Rev. Accel. Beams 22 (2019) 041304, http://dx.doi.org/10.1103/PhysRevAccelBeams.22.041304, URL https://link.aps.org/doi/10.1103/PhysRevAccelBeams.22.041304.

[19] Y. Zhao, W. An, X. Xu, F. Li, L. Hildebrand, M.J. Hogan, V. Yakimenko, C. Joshi, W.B. Mori, Emittance preservation through density ramp matching sections in a plasma wakefield accelerator, Phys. Rev. Accel. Beams 23 (2020) 011302, http://dx.doi.org/10.1103/PhysRevAccelBeams.23.011302, URL https://link.aps.org/doi/10.1103/PhysRevAccelBeams.23.011302.

[20] D.H. Whittum, W.M. Sharp, S.S. Yu, M. Lampe, G. Joyce, Electron-hose instability in the ion-focused regime, Phys. Rev. Lett. 67 (1991) 991–994, http://dx.doi.org/10.1103/PhysRevLett.67.991, URL https://link.aps.org/doi/10.1103/PhysRevLett.67.991.

[21] T.J. Mehrling, R.A. Fonseca, A. Martinez de la Ossa, J. Vieira, Mitigation of the hose instability in plasma-wakefield accelerators, Phys. Rev. Lett. 118 (2017) 174801, http://dx.doi.org/10.1103/PhysRevLett.118.174801, URL https://link.aps.org/doi/10.1103/PhysRevLett.118.174801.

[22] A. Martinez de la Ossa, T.J. Mehrling, J. Osterhoff, Intrinsic stabilization of the drive beam in plasma-wakefield accelerators, Phys. Rev. Lett. 121 (2018) 064803, http://dx.doi.org/10.1103/PhysRevLett.121.064803, URL https://link.aps.org/doi/10.1103/PhysRevLett.121.064803.

[23] E.L. Saldin, E.A. Schneidmiller, M.V. Yurkov, On the coherent radiation of an electron bunch moving in an arc of a circle, Nucl. Instrum. Methods Phys. Res. A (ISSN: 0168-9002) 398 (2) (1997) 373–394, http://dx.doi.org/10.1016/S0168-9002(97)00822-X, URL https://www.sciencedirect.com/science/article/pii/S016890029700822X.

[24] M. Litos, E. Adli, W. An, C.I. Clarke, C.E. Clayton, S. Corde, J.P. Delahaye, R.J. England, A.S. Fisher, J. Frederico, S. Gessner, S.Z. Green, M.J. Hogan, C. Joshi, W. Lu, K.A. Marsh, W.B. Mori, P. Muggli, N. Vafaei-Najafabadi, D. Walz, G. White, Z. Wu, V. Yakimenko, G. Yocky, High-efficiency acceleration of an electron beam in a plasma wakefield accelerator, Nature 515 (2014) 92, http://dx.doi.org/10.1038/nature13882.

[25] M.J. Hogan, T.O. Raubenheimer, A. Seryi, P. Muggli, T. Katsouleas, C. Huang, W. Lu, W. An, K.A. Marsh, W.B. Mori, C.E. Clayton, C. Joshi, Plasma wakefield acceleration experiments at FACET, New J. Phys. 12 (5) (2010) 055030, http://dx.doi.org/10.1088/1367-2630/12/5/055030.

[26] R. D'Arcy, A. Aschikhin, S. Bohlen, G. Boyle, T. Brümmer, J. Chappell, S. Diederichs, B. Foster, M.J. Garland, L. Goldberg, P. Gonzalez, S. Karstensen, A. Knetsch, P. Kuang, V. Libov, K. Ludwig, A. Martinez de la Ossa, F. Marutzky, M. Meisel, T.J. Mehrling, P. Niknejadi, K. Põder, P. Pourmoussavi, M. Quast, J.H. Röckemann, L. Schaper, B. Schmidt, S. Schröder, J.P. Schwinkendorf, B. Sheeran, G. Tauscher, S. Wesch, M. Wing, P. Winkler, M. Zeng, J. Osterhoff, Flashforward: plasma wakefield accelerator science for high-average-power applications, Philos. Trans. R. Soc. A 377 (2151) (2019) 20180392, http://dx.doi.org/10.1098/rsta.2018.0392, URL https://royalsocietypublishing.org/doi/abs/10.1098/rsta.2018.0392.

[27] S. Schröder, C.A. Lindstrøm, S. Bohlen, G. Boyle, R. D'Arcy, S. Diederichs, M.J. Garland, P. Gonzalez, A. Knetsch, V. Libov, P. Niknejadi, K. Põder, L. Schaper, B. Schmidt, B. Sheeran, G. Tauscher, S. Wesch, J. Zemella, M. Zeng, J. Osterhoff, High-resolution sampling of beam-driven plasma wakefields, Nature Commun. 11 (2020) 5984, http://dx.doi.org/10.1038/s41467-020-19811-9.

[28] Y. Ding, C. Behrens, R. Coffee, F.-J. Decker, P. Emma, C. Field, W. Helml, Z. Huang, P. Krejcik, J. Krzywinski, H. Loos, A. Lutman, A. Marinelli, T.J. Maxwell, J. Turner, Generating femtosecond X-ray pulses using an emittance-spoiling foil in free-electron lasers, Appl. Phys. Lett. 107 (19) (2015) 191104, http://dx.doi.org/10.1063/1.4935429.

[29] A. Marinelli, D. Ratner, A. Lutman, J. Turner, J. Welch, F.-J. Decker, H. Loos, C. Behrens, S. Gilevich, A. Miahnahri, S. Vetter, T. Maxwell, Y. Ding, R. Coffee, S. Wakatsuki, Z. Huang, High-intensity double-pulse X-ray free-electron laser, Nature Commun. 6 (1) (2015) 6369, http://dx.doi.org/10.1038/ncomms7369.

[30] Z. Zhang, Y. Ding, A. Marinelli, Z. Huang, Longitudinal dynamics of twin electron bunches in the linac coherent light source, Phys. Rev. ST Accel. Beams 18 (2015) 030702, http://dx.doi.org/10.1103/PhysRevSTAB.18.030702, URL https://link.aps.org/doi/10.1103/PhysRevSTAB.18.030702.

[31] J. Björklund Svensson, H. Ekerfelt, O. Lundh, T.K. Charles, J. Andersson, M. Kotur, F. Lindau, E. Mansten, S. Thorin, Beamline design for plasma-wakefield acceleration experiments at MAX IV, in: Proc. AAC '18, 2018, http://dx.doi.org/10.1109/AAC.2018.8659401, URL https://ieeexplore.ieee.org/abstract/document/8659401.

[32] J. Björklund Svensson, H. Ekerfelt, O. Lundh, J. Andersson, F. Curbis, M. Kotur, F. Lindau, E. Mansten, S. Thorin, S. Werin, Driver-witness-bunches for plasma-wakefield acceleration at the max IV linear accelerator, in: Proc. IPAC'17, 2017, TUPIK031 URL https://accelconf.web.cern.ch/ipac2017/papers/tupik031.pdf.

[33] S. Thorin, J. Andersson, F. Curbis, M. Eriksson, O. Karlberg, D. Kumbaro, E. Mansten, D. Olsson, S. Werin, The MAX IV linac, in: Proc. LINAC'14, 2014, TUIOA03 URL https://accelconf.web.cern.ch/LINAC2014/papers/tuioa03.pdf.

[34] S.C. Leemann, Å. Andersson, M. Eriksson, L.-J. Lindgren, E. Wallén, J. Bengtsson, A. Streun, Beam dynamics and expected performance of Sweden's new storage-ring light source: MAX IV, Phys. Rev. ST Accel. Beams 12 (12) (2009) 120701, http://dx.doi.org/10.1103/PhysRevSTAB.12.120701, URL https://link.aps.org/doi/10.1103/PhysRevSTAB.12.120701.

[35] S. Werin, S. Thorin, M. Eriksson, J. Larsson, Short pulse facility for MAX-lab, Nucl. Instrum. Methods Phys. Res. A 601 (1–2) (2009) 98–107, http://dx.doi.org/10.1016/j.nima.2008.12.106, URL https://www.sciencedirect.com/science/article/pii/S0168900208020160.

[36] S. Werin, J. Andersen, P.F. Tavares, L. Isaksson, M. Kotur, F. Lindau, E. Mansten, D. Olsson, H. Tarawneh, S. Thorin, F. Curbis, V. Goryashko, S. Bonetti, M. Larsson, A. Nilsson, P. Salén, P. Johnsson, The soft X-ray laser project at MAX IV, in: Proc. IPAC'17, 2017, WEPAB077 URL https://accelconf.web.cern.ch/ipac2017/papers/wepab077.pdf.

[37] W. Qin, F. Curbis, J. Andersson, V. Goryashko, L. Isaksson, B. Kyle, F. Lindau, E. Mansten, M. Pop, P. Salén, H. Tarawneh, P.F. Tavares, S. Thorin, A. Vorozhtsov, S. Werin, The FEL in the SXL project at MAX IV, J. Synchrotron Radiat. 28 (3) (2021) 707–717, http://dx.doi.org/10.1107/S1600577521003465.

[38] A. Vorozhtsov, A. Nilsson, A. Rosborg, A. Johansson, B. Kyle, C. Weninger, D. Olsson, D. Kumbaro, D. Alj, E. Hillner, E. Mansten, E. Al-Dmour, F. Maia, F. Lindau, F. Curbis, G.P. Segurana, H. Tarawneh, I. Bailey, J.-E. Rubensson, J. Koliyadu, J. Andersson, J.B. Svensson, J. Breunlin, J. Modéer, J. Sellberg, L. Isaksson, L. Roslund, M. Grabski, M. Agåker, M. Brandin, M. Larsson, M. Holz, M. Pop, M. Eriksson, M. Ebbeni, M. Gehlot, P.F. Tavares, P. Eng-Johnsson, P. Lilja, P. Salén, P. Williams, R. Lindvall, R. Svärd, S. Pirani, S. Thorin, S. Benedictsson, S. Bonetti, S. Molloy, S. Werin, S. Maclot, V. Goryashko, W. Qin, Y. Feng, The soft X-ray laser at MAX IV - conceptual design report, Tech. rep., MAX IV Laboratory, 2021, URL https://www.maxiv.lu.se/soft-x-ray-laser/.

[39] J. Andersson, F. Curbis, D. Kumbaro, F. Lindau, S. Werin, Beam performance of the photocathode gun for the MAX IV linac, in: Proc. FEL'14, 2014, THP037 URL https://accelconf.web.cern.ch/FEL2014/papers/thp037.pdf.

[40] F. Lindau, J. Andersson, J. Björklund Svensson, M. Brandin, F. Curbis, M. Kotur, D. Kumbaro, E. Mansten, L. Isaksson, D. Olsson, R. Svärd, S. Thorin, S. Werin, MAX IV photocathode gun laser system specification and diagnostics, in: Proc. IPAC'17, 2017, TUPAB097 URL https://accelconf.web.cern.ch/ipac2017/papers/tupab097.pdf.

[41] M. Kotur, J. Andersson, J. Björklund Svensson, M. Brandin, F. Curbis, F. Lindau, D. Kumbaro, E. Mansten, L. Isaksson, D. Olsson, R. Svärd, S. Thorin, S. Werin, Pulse shaping at the MAX IV photoelectron gun laser, in: Proc. IPAC'17, 2017, TUPAB096 URL https://accelconf.web.cern.ch/ipac2017/papers/tupab096.pdf.

[42] S. Thorin, M. Eriksson, S. Werin, D. Angal-Kalinin, J. McKenzie, B. Militsyn, P. Williams, Bunch compression by linearising achromats for the MAX IV injector, in: Proc. FEL'10, 2010, WEPB34 URL https://accelconf.web.cern.ch/FEL2010/papers/wepb34.pdf.

[43] FemtoMAX, 2021, URL https://www.maxiv.lu.se/accelerators-beamlines/beamlines/femtomax/.

[44] D. Olsson, F. Curbis, E. Mansten, S. Thorin, S. Werin, Transverse RF deflecting structures for the MAX IV linac, in: Proc. IPAC'18, 2018, THPAL027 URL https://accelconf.web.cern.ch/ipac2018/papers/thpal027.pdf.

[45] P. Craievich, M. Bopp, H.-H. Braun, A. Citterio, R. Fortunati, R. Ganter, T. Kleeb, F. Marcellini, M. Pedrozzi, E. Prat, S. Reiche, K. Rolli, R. Sieber, A. Grudiev, W.L. Millar, N. Catalan-Lasheras, G. McMonagle, S. Pitman, V.d.P. Romano, K.T. Szypula, W. Wuensch, B. Marchetti, R. Assmann, F. Christie, B. Conrad, R. D'Arcy, M. Foese, P.G. Caminal, M. Hoffmann, M. Huening, R. Jonas, O. Krebs, S. Lederer, D. Marx, J. Osterhoff, M. Reukauff, H. Schlarb, S. Schreiber, G. Tews, M. Vogt, A.d.Z. Wagner, S. Wesch, Novel X-band transverse deflection structure with variable polarization, Phys. Rev. Accel. Beams 23 (2020) 112001, http://dx.doi.org/10.1103/PhysRevAccelBeams.23.112001, URL https://link.aps.org/doi/10.1103/PhysRevAccelBeams.23.112001.

[46] B. Marchetti, A. Grudiev, P. Craievich, R. Assmann, H.-H. Braun, N. Catalan Lasheras, F. Christie, R. D'Arcy, R. Fortunati, R. Ganter, P. González Caminal, M. Hoffmann, M. Huening, S.M. Jaster-Merz, R. Jonas, F. Marcellini, D. Marx, G. McMonagle, J. Osterhoff, M. Pedrozzi, E. Prat Costa, S. Reiche, M. Reukauff, S. Schreiber, G. Tews, M. Vogt, S. Wesch, W. Wuensch, Experimental demonstration of novel beam characterization using a polarizable X-band transverse deflection structure, Sci. Rep. 11 (1) (2021) 3560, http://dx.doi.org/10.1038/s41598-021-82687-2.

[47] K. Floettmann, ASTRA User Manual, 2000.

[48] F. Zhou, A. Brachmann, P. Emma, S. Gilevich, Z. Huang, Impact of the spatial laser distribution on photocathode gun operation, Phys. Rev. ST Accel. Beams 15 (2012) 090701, http://dx.doi.org/10.1103/PhysRevSTAB.15.090701, URL https://link.aps.org/doi/10.1103/PhysRevSTAB.15.090701.

[49] L. Serafini, The short bunch blow-out regime in RF photoinjectors, AIP Conf. Proc. 413 (1) (1997) 321–334, http://dx.doi.org/10.1063/1.54425, URL https://aip.scitation.org/doi/abs/10.1063/1.54425.

[50] O.J. Luiten, S.B. van der Geer, M.J. de Loos, F.B. Kiewiet, M.J. van der Wiel, How to realize uniform three-dimensional ellipsoidal electron bunches, Phys. Rev. Lett. 93 (2004) 094802, http://dx.doi.org/10.1103/PhysRevLett.93.094802, URL https://link.aps.org/doi/10.1103/PhysRevLett.93.094802.

[51] M. Borland, Elegant: A flexible SDDS-compliant code for accelerator simulation, Tech. rep., Argonne National Lab., IL (US), 2000.

[52] J. Björklund Svensson, T.K. Charles, O. Lundh, S. Thorin, Third-order double-achromat bunch compressors for broadband beams, Phys. Rev. Accel. Beams 22 (2019) 104401, http://dx.doi.org/10.1103/PhysRevAccelBeams.22.104401, URL https://link.aps.org/doi/10.1103/PhysRevAccelBeams.22.104401.

[53] E. Lefebvre, N. Cochet, S. Fritzler, V. Malka, M.-M. Aléonard, J.-F. Chemin, S. Darbon, L. Disdier, J. Faure, A. Fedotoff, O. Landoas, G. Malka, V. Méot, P. Morel, M. Rabec Le Gloahec, A. Rouyer, C. Rubbelynck, V. Tikhonchuk, R. Wrobel, P. Audebert, C. Rousseaux, Electron and photon production from relativistic laser-plasma interactions, Nucl. Fusion 43 (7) (2003) 629–633, http://dx.doi.org/10.1088/0029-5515/43/7/317.

[54] X. Davoine, Laser-driven wakefield electron acceleration and associated radiation sources (Ph.D. thesis), Universite de Versailles-Saint-Quentin-en-Yvelines, 2009, FRCEA-TH–1780 URL http://inis.iaea.org/search/search.aspx?orig_q=RN:42013895.

[55] K.L.F. Bane, P. Chen, P.B. Wilson, On collinear wake field acceleration, IEEE Trans. Nucl. Sci. 32 (5) (1985) 3524–3526, http://dx.doi.org/10.1109/TNS.1985.4334416,.

[56] J.B. Rosenzweig, B. Breizman, T. Katsouleas, J.J. Su, Acceleration and focusing of electrons in two-dimensional nonlinear plasma wake fields, Phys. Rev. A 44 (1991) R6189–R6192, http://dx.doi.org/10.1103/PhysRevA.44.R6189, URL https://link.aps.org/doi/10.1103/PhysRevA.44.R6189.

[57] G. Loisch, G. Asova, P. Boonpornprasert, R. Brinkmann, Y. Chen, J. Engel, J. Good, M. Gross, F. Grüner, H. Huck, D. Kalantaryan, M. Krasilnikov, O. Lishilin, A.M. de la Ossa, T.J. Mehrling, D. Melkumyan, A. Oppelt, J. Osterhoff, H. Qian, Y. Renier, F. Stephan, C. Tenholt, V. Wohlfarth, Q. Zhao, Observation of high transformer ratio plasma wakefield acceleration, Phys. Rev. Lett. 121 (2018) 064801, http://dx.doi.org/10.1103/PhysRevLett.121.064801, URL https://link.aps.org/doi/10.1103/PhysRevLett.121.064801.

[58] J. Andersson, J. Björklund Svensson, M. Kotur, F. Lindau, S. Thorin, Creating two-pulse beams from a photoinjector for two color FEL or beam driven PWFA experiments, in: Proc. IPAC'18, 2018, THPMK001 URL https://accelconf.web.cern.ch/ipac2018/papers/thpmk001.pdf.

[59] A.D. Brynes, P. Smorenburg, I. Akkermans, E. Allaria, L. Badano, S. Brussaard, M. Danailov, A. Demidovich, G. De Ninno, D. Gauthier, G. Gaio, S.B. van der Geer, L. Giannessi, M.J. de Loos, N.S. Mirian, G. Penco, P. Rebernik, F. Rossi, I. Setija, S. Spampinati, C. Spezzani, M. Trovò, P.H. Williams, S. Di Mitri, Beyond the limits of 1D coherent synchrotron radiation, New J. Phys. 20 (7) (2018) 073035, http://dx.doi.org/10.1088/1367-2630/aad21d.

[60] A.D. Brynes, P. Smorenburg, I. Akkermans, E. Allaria, L. Badano, S. Brussaard, M. Danailov, A. Demidovich, G.D. Ninno, D. Gauthier, G. Gaio, S.B. van der Geer, L. Giannessi, M.J. de Loos, N.S. Mirian, G. Penco, P. Rebernik, F. Rossi, I. Setija, S. Spampinati, C. Spezzani, M. Trovò, P.H. Williams, S.D. Mitri, Addendum: Beyond the limits of 1D coherent synchrotron radiation (2018 new J. Phys. 20 073035), New J. Phys. 23 (4) (2021) 049401, http://dx.doi.org/10.1088/1367-2630/abed6c.

[61] P. Muggli, K.A. Marsh, S. Wang, C.E. Clayton, S. Lee, T.C. Katsouleas, C. Joshi, Photo-ionized lithium source for plasma accelerator applications, IEEE Trans. Plasma Sci. 27 (3) (1999) 791–799, http://dx.doi.org/10.1109/27.774685.

[62] S.Z. Green, E. Adli, C.I. Clarke, S. Corde, S.A. Edstrom, A.S. Fisher, J. Frederico, J.C. Frisch, S. Gessner, S. Gilevich, P. Hering, M.J. Hogan, R.K. Jobe, M. Litos, J.E. May, D.R. Walz, V. Yakimenko, C.E. Clayton, C. Joshi, K.A. Marsh, N. Vafaei-Najafabadi, P. Muggli, Laser ionized preformed plasma at FACET, Plasma Phys. Control. Fusion 56 (8) (2014) 084011, http://dx.doi.org/10.1088/0741-3335/56/8/084011.

[63] G. Plyushchev, R. Kersevan, A. Petrenko, P. Muggli, A rubidium vapor source for a plasma source for AWAKE, J. Phys. D 51 (2) (2017) 025203, http://dx.doi.org/10.1088/1361-6463/aa9dd7.

[64] D.J. Spence, A. Butler, S.M. Hooker, Gas-filled capillary discharge waveguides, J. Opt. Soc. Amer. B 20 (1) (2003) 138–151, http://dx.doi.org/10.1364/JOSAB.20.000138, URL http://opg.optica.org/josab/abstract.cfm?URI=josab-20-1-138.

[65] K.V. Lotov, Efficient operating mode of the plasma wakefield accelerator, Phys. Plasmas 12 (053105) (2005) http://dx.doi.org/10.1063/1.1889444.

[66] W.H. Tan, P. Piot, A. Zholents, Formation of temporally shaped electron bunches for beam-driven collinear wakefield accelerators, Phys. Rev. Accel. Beams 24 (2021) 051303, http://dx.doi.org/10.1103/PhysRevAccelBeams.24.051303, URL https://link.aps.org/doi/10.1103/PhysRevAccelBeams.24.051303.

[67] P. Emma, M. Venturini, K.L.F. Bane, G. Stupakov, H.-S. Kang, M.S. Chae, J. Hong, C.-K. Min, H. Yang, T. Ha, W.W. Lee, C.D. Park, S.J. Park, I.S. Ko, Experimental demonstration of energy-chirp control in relativistic electron bunches using a corrugated pipe, Phys. Rev. Lett. 112 (2014) 034801, http://dx.doi.org/10.1103/PhysRevLett.112.034801, URL https://link.aps.org/doi/10.1103/PhysRevLett.112.034801.

[68] S. Antipov, S. Baturin, C. Jing, M. Fedurin, A. Kanareykin, C. Swinson, P. Schoessow, W. Gai, A. Zholents, Experimental demonstration of energy-chirp compensation by a tunable dielectric-based structure, Phys. Rev. Lett. 112 (2014) 114801, http://dx.doi.org/10.1103/PhysRevLett.112.114801, URL https://link.aps.org/doi/10.1103/PhysRevLett.112.114801.

[69] R. D'Arcy, S. Wesch, A. Aschikhin, S. Bohlen, C. Behrens, M.J. Garland, L. Goldberg, P. Gonzalez, A. Knetsch, V. Libov, A.M. de la Ossa, M. Meisel, T.J. Mehrling, P. Niknejadi, K. Poder, J.-H. Röckemann, L. Schaper, B. Schmidt, S. Schröder, C. Palmer, J.-P. Schwinkendorf, B. Sheeran, M.J.V. Streeter, G. Tauscher, V. Wacker, J. Osterhoff, Tunable plasma-based energy dechirper, Phys. Rev. Lett. 122 (2019) 034801, http://dx.doi.org/10.1103/PhysRevLett.122.034801, URL https://link.aps.org/doi/10.1103/PhysRevLett.122.034801.

[70] P. Wilson, Introduction to Wakefields and Wake Potentials, Tech. Rep. PUB-4547, SLAC, 1989.

[71] O. Karlberg, F. Curbis, S. Thorin, S. Werin, Characterization of longitudinal wakefields in the MAX IV linac, in: Proc. IPAC'14, 2014, THPRO074 URL https://accelconf.web.cern.ch/IPAC2014/papers/thpro074.pdf.

[72] O. Karlberg, F. Curbis, S. Werin, S. Thorin, P. Craievich, G. Penco, E. Ferrari, Short range wakefields in MAX IV and FERMI linac, in: Proc. IPAC'12, 2012, WEPPR060 URL https://accelconf.web.cern.ch/IPAC2012/papers/weppr060.pdf.

[73] C.A. Lindstrøm, E. Adli, Design of general apochromatic drift-quadrupole beam lines, Phys. Rev. Accel. Beams 19 (2016) 071002, http://dx.doi.org/10.1103/PhysRevAccelBeams.19.071002, URL https://link.aps.org/doi/10.1103/PhysRevAccelBeams.19.071002.

[74] J. van Tilborg, S. Steinke, C.G.R. Geddes, N.H. Matlis, B.H. Shaw, A.J. Gonsalves, J.V. Huijts, K. Nakamura, J. Daniels, C.B. Schroeder, C. Benedetti, E. Esarey, S.S. Bulanov, N.A. Bobrova, P.V. Sasorov, W.P. Leemans, Active plasma lensing for relativistic laser-plasma-accelerated electron beams, Phys. Rev. Lett. 115 (2015) 184802, http://dx.doi.org/10.1103/PhysRevLett.115.184802, URL https://link.aps.org/doi/10.1103/PhysRevLett.115.184802.

[75] C.A. Lindstrøm, E. Adli, G. Boyle, R. Corsini, A.E. Dyson, W. Farabolini, S.M. Hooker, M. Meisel, J. Osterhoff, J.-H. Röckemann, L. Schaper, K.N. Sjobak, Emittance preservation in an aberration-free active plasma lens, Phys. Rev. Lett. 121 (2018) 194801, http://dx.doi.org/10.1103/PhysRevLett.121.194801, URL https://link.aps.org/doi/10.1103/PhysRevLett.121.194801.

[76] C.E. Doss, E. Adli, R. Ariniello, J. Cary, S. Corde, B. Hidding, M.J. Hogan, K. Hunt-Stone, C. Joshi, K.A. Marsh, J.B. Rosenzweig, N. Vafaei-Najafabadi, V. Yakimenko, M. Litos, Laser-ionized, beam-driven, underdense, passive thin plasma lens, Phys. Rev. Accel. Beams 22 (2019) 111001, http://dx.doi.org/10.1103/PhysRevAccelBeams.22.111001, URL https://link.aps.org/doi/10.1103/PhysRevAccelBeams.22.111001.